J. Appl. Comput. Mech., 7(2) (2021) 820-830
DOI: 10.22055/JACM.2020.35968.2771

ISSN: 2383-4536
jacm.scu.ac.ir

Shahid Chamran University of Ahvaz

Journal of Applied and Computational Mechanics

Research Paper

Finite Element and Experimental Investigation on the Effect of Repetitive Shock in Corrugated Cardboard Packaging

Viet Dung Luong[1], Anne-Sophie Bonnin[2], Fazilay Abbès[1], Jean-Baptiste Nolot[2], Damien Erre[2], Boussad Abbès[1]

[1] MATIM, University of Reims Champagne-Ardenne, UFR SEN, Campus Moulin de la Housse, 51100 Reims, France

[2] ESIReims, University of Reims Champagne-Ardenne, Esplanade Roland Garros, 51100 Reims, France

Received December 05 2020; Revised December 26 2020; Accepted for publication December 27 2020.
Corresponding author: B. Abbès (boussad.abbes@univ-reims.fr)

Abstract. The primary concern of the current study is estimating the repetitive shock induced damages leading to cumulative fatigue on corrugated cardboard boxes experimentally and numerically. Repetitive shock tests were performed on boxes using a vibration table to construct a Damage Boundary Curve (DBC). To computationally determine this curve, a finite element approach is proposed using an elastoplastic homogenization model for corrugated cardboard. The proposed model was implemented in the finite element software ABAQUS. Thanks to adopted model simplifications, a box can be easily and reliably modelled as a homogenized structure. A calibration method is used to compute a set of effective parameters in homogenized model in order to keep its behavior qualitatively and quantitatively close to the response of a full structural model. For verification, the identified model is used to simulate the box compression test. To replicate the experimental tests, simulations of successive repetitive shock pulses are carried with the proposed model for oligocyclique and limited endurance fatigue. To reduce computational costs, we propose a simple method for unlimited endurance fatigue by extrapolating a trend line after some training cycles. The proposed method shows good agreement with experimental results.

Keywords: Packaging, Shock test, Fatigue, Finite element simulation, Elastoplastic model.

1. Introduction

Corrugated cardboard boxes are designed to protect products from hazards of the distribution, transportation, and storage environment so that the products can be shipped to consumers without damage. When packaged products are shipped, they may encounter many dynamic events such as drops, impacts, compressions, vibrations…etc. during handling and transportation which might cause damage to the product. Shocks are one of the most severe factors that cause damage to products. The intensity of a given shock is characterized by its acceleration level or amplitude, and the duration over which the shock takes place [1]. Another important characterization of a shock pulse is the velocity change, which is represented by the area under the acceleration amplitude versus time curve. The damage boundary curve (DBC) is widely used to determine the shock damage of a product based on its sensitivity to acceleration and velocity change [2]. DBCs were applied to evaluate repetitive-shock-induced damage [3-5]. Test procedure to determine DBC usually requires the use of a programmable shock machine, which can vary the amplitude, duration and velocity change parameters of repeated impacts [6-9]. In our study, a test procedure is proposed using a vibration table to generate shocks of various shapes and intensities to construct the DBC of a corrugated cardboard box.

Finite element (FE) modelling of corrugated cardboard has been an area of extensive research in static analysis. Biancolini et al. [10-11] developed equivalent material models of corrugated cardboard using a homogenization approach to predict the eigenvalue buckling load, and ultimate compression load from nonlinear static analyses of boxes. Han and Park [12] and Fadiji et al. [13] investigated the effects of vent design on compression strength using FE simulations on ventilated corrugated cardboard boxes. FE modelling of corrugated cardboard packages is fastidious, and the meshing generates heavy models which increases CPU time. In order to deal with this, researchers developed homogenization models that replace 3D structural models with a single-layered shell model. The proposed homogenization methods generally deal only with elastic properties [14-18], while for the description of nonlinear behavior of corrugated cardboard also plasticity must be considered [7, 19]. Rabczuk et al. [20] proposed a homogenization method for sandwich structures based on the equivalence of the continuum stored energy density function and a discrete energy associated to a representative core cell considering material nonlinearities including buckling of the core. They applied this homogenization to different types of cores under dynamic loading and in fluid–structure interaction examples. Recently, Anitescu et al. [21] proposed a method based on artificial neural networks (ANN) and an adaptive collocation strategy that can be applied for such problems. To model the orthotropic plastic behavior of paperboard, the common plasticity models used for are Hill [22], Hoffman [23], Tsai and Wu [24], Xia et al. [25], Mäkelä and Östlund [26], Harrysson and Ristinmaa [27]. Since corrugated cardboard consists of flat paperboard layers (linerboards) distanced by sine-shaped layer (fluting), the determination of effective elastoplastic

Published online: December 28 2020

parameters for shell model that replaces 3D structural corrugated cardboard model is not an easy task. An inverse identification procedure can be used to calibrate effective elastoplastic parameters [7, 19].

The main concern of this study is estimating the effect of repetitive shock on corrugated cardboard boxes. Novelty of this study is the construction of the Damage Boundary Curve (DBC) using a vibration table and a finite element approach with an elastoplastic homogenization model for corrugated cardboard.

2. Material and Methods

In this section, we present the corrugated cardboard and the experimental techniques used in this study. To determine the material parameters, we carried out tensile tests on the papers constituting the corrugated cardboard. Corrugated cardboard boxes were then tested to study their behavior in compression and under repetitive shock leading to cumulative fatigue.

2.1 Corrugated Cardboard

For this study, we have used a single wall corrugated cardboard material consisting of a fluted corrugated sheet and two flat linerboards (Fig. (1)). The thickness and grammage (weight per meter square) of each constituent are given in Table (1). The corrugated cardboard was immersed in water to separate the sheets. The peeled off sheets were wrung by pressing them between absorbent papers before their conditioning at 23°C and 50% relative humidity (RH) for two days.

2.2 Tensile Tests

Using a cutting table (ZÜND M-1600), we cut ten standard specimens from the constituents of the corrugated cardboard to perform tensile tests in three directions (MD, CD and 45°). To ensure a better grip of the clamps when tightening these specimens, we glued pieces of rigid compact cardboard to both ends.

The tensile tests were performed on an MTS Adamel-Lhomargy DY35XL testing machine equipped with 2 kN load cell. The standard test to evaluate a paperboard's tensile properties was conducted on a 10 mm wide specimen that was clamped with a free span of 100 mm. The specimen was deformed at a constant rate of 10 mm/min while the force is recorded. To minimize the influence of climatic conditions, all tests were performed at 23°C and 50% RH.

2.3 Box Compression Test

Corrugated cardboard boxes are often stacked on one another to certain layers to form pallets. The box must have the capacity to bear the load during storage and transport. It is thus important to check the compression strength of the box. The box compression strength is a direct measure of its stacking strength.

Figure (2) shows the unfolded box with dimensions LxWxH = 300x200x180 mm^3. The box is compressed at a constant rate of 10 mm/min between two rigid platens. The platens are fixed so that they remain parallel on an INSTRON 4204 testing machine equipped with a 5 kN load cell. The compression tests were carried out under standard conditions at 23°C and 50% RH.

2.4 Repetitive Shock Experiments

Corrugated cardboard boxes are used to protect their contents from the hazards encountered in handling, transportation, and storage. These packages are at risk of being dropped or damaged during handling and shipping. Shock is one of the more troublesome of these hazards. Shock testing techniques are used to identify the vulnerabilities of engineered products and components. Controlled shock input by shock machines provides a convenient method for evaluating the ability of shipping containers to withstand shocks.

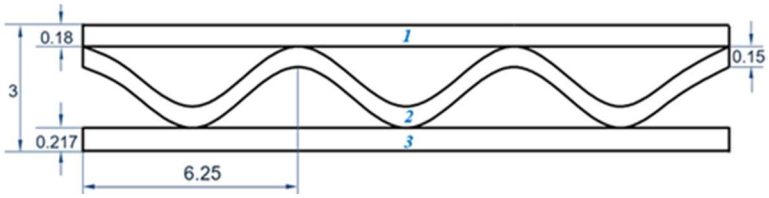

Fig. 1. Geometry and dimensions of flute B corrugated cardboard.

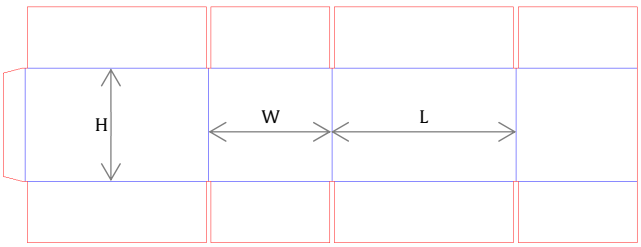

Fig. 2. Unfolded box.

Table 1. Thickness and grammage of flute B corrugated cardboard.

	Thickness (mm)	Grammage (g/m^2)
Top linerboard	0.180±0.004	140
Fluting	0.150±0.008	113
Bottom linerboard	0.217±0.004	130

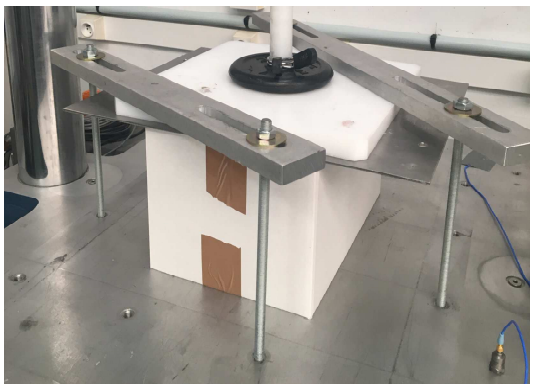

Fig. 3. Experimental setup for shock testing on the vibration table.

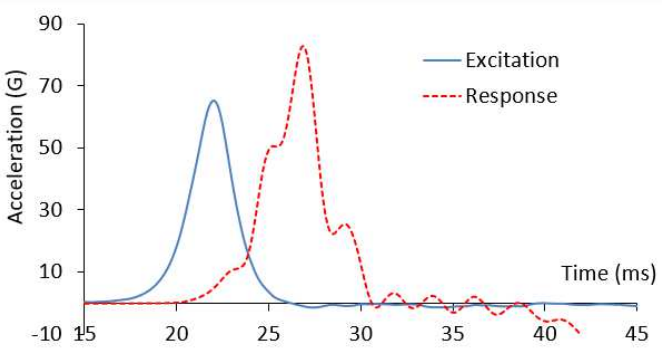

Fig. 4. Example of a half-sine shock pulse and corresponding response.

Shock tests were performed on the same boxes introduced in previous section using a servo-hydraulic vibration table connected to a real-time vibration controller (SEREME, France) programmed to generate shocks of various shapes and intensities. As in most mechanical shock test procedures, fixturing of the package on the shock test machine may have significant influence on the test results. In this study, the box is fixed on the vibration table by a structure consisting of link bars connected to the table by bolts as shown in Fig. (3). The box is preloaded with a total mass of 8.4 kg.

The test procedure for repetitive shock experiment is as follows: the vibration table generates a shock in the vertical direction and the response of the system shown in Fig. (4) is recorded. A box is subjected to repetitive shock with the same intensity until a visible damage is observed on the box. The damaged box is then removed and replaced by a new one to undergo a series of shocks with another level of intensity. The acceleration and velocity change are the two parameters recorded and plotted in the testing procedure. With this procedure, we obtain the Damage Boundary Curve (DBC) which is constructed from the critical acceleration and the critical velocity change when the box is damaged.

3. Material Model

To efficiently simulate the mechanical behavior of a corrugated cardboard box, we need to use a homogenization model instead using the full 3D model to reduce the preparation of the model and the computational times. The homogenization consists in representing the corrugated-core sandwich panel by a homogeneous plate.

3.1 Governing equations

The dynamic boundary value problem (BVP) in a 3D cartesian frame is written in a strong form as:

$$\rho \ddot{u}_i = \sigma_{ij,j} + f_i \tag{1}$$

where u_i are the displacement vector components, ρ is the density value, σ_{ij} are the stress tensor components, and f_i are the body force components.

The kinematic relations for the strain rates are given as follows:

$$\dot{\varepsilon}_{ij} = \frac{1}{2}\left(\dot{u}_{i,j} + \dot{u}_{j,i}\right) = \dot{\varepsilon}^e_{ij} + \dot{\varepsilon}^p_{ij} \tag{2}$$

where ε_{ij} are the strain tensor components, ε^e_{ij} and ε^p_{ij} are the components of the elastic and plastic strain tensors.

The constitutive equations relating stress rates and elastic strain rates are given by:

$$\dot{\sigma}_{ij} = C_{ijkl}\dot{\varepsilon}^e_{kl} \tag{3}$$

where C_{ijkl} is the matrix of elastic moduli.

Considering the decomposition of the strain rate tensor into elastic and plastic components, the Hooke's law is written in the following form:

$$\dot{\sigma}_{ij} = C_{ijkl}\left(\dot{\varepsilon}_{kl} - \dot{\varepsilon}^p_{kl}\right) \tag{4}$$

The boundary conditions set on the S_v and S_σ surfaces, respectively, are:

$$\begin{cases} \dot{u}_i = v_i, & on\ S_v \\ \sigma_{ij} n_j = T_i, & on\ S_\sigma \end{cases} \tag{5}$$

where v_i is the loading velocity, T_i is the traction and n_i is the surface normal.

3.2 Paperboard Elastoplastic Model

In this work, the orthotropic elastoplastic material model proposed by Mäkelä and Östlund [26] was used to predict the behavior of the linerboards and the fluting. This model is based on the concept of material equivalent isotropic plasticity (IPE) introduced by Karafillis and Boyce [28]. The IPE-material is a fictitious isotropic material, subjected to a stress state that equals the corresponding stress state in the actual anisotropic material.

The yield criterion may be expressed as:

$$f = \sigma_{eq} - \sigma_y = \left(\frac{3}{2}\{s\}\{s\}\right)^{1/2} - E_0\left(\varepsilon_0 + \varepsilon_{eq}^p\right)^{1/n} \tag{6}$$

where σ_y is the yield stress, $\{s\}$ is the deviatoric stress tensor, ε_{eq}^p is the equivalent plastic strain, E_0 and ε_0, are two model parameters.

However, the definition of the deviatoric stress tensor for the IPE-material differs from J2-flow theory and is expressed as:

$$\{s\} = \begin{Bmatrix} s_x \\ s_y \\ s_z \\ s_{xy} \end{Bmatrix} = [L]\{\sigma\} = \frac{1}{3}\begin{bmatrix} 2a & c-a-b & 0 \\ c-a-b & 2b & 0 \\ b-c-a & a-b-c & 0 \\ 0 & 0 & 3d \end{bmatrix} \begin{Bmatrix} \sigma_x \\ \sigma_y \\ \sigma_{xy} \end{Bmatrix} \tag{7}$$

where a, b, c and d are model parameters.

Since this material model is not available in ABAQUS software, it was implemented using the material user subroutine VUMAT [29]. The aim of this material subroutine is to invoke a given increment in total strain and return the corresponding stress state and the internal state variable (the equivalent plastic strain in our case). A backward-Euler approach is adopted in the implementation of the subroutine.

The starting point of the calculation of the stress state, corresponding to a given increment in total strain $\Delta\varepsilon_{ij}$, is the calculation of the trial stress state $\sigma_{ij}^{tr}{}_{new}$ assuming a pure elastic behavior:

$$\sigma_{ij}^{tr}{}_{new} = \sigma_{ij}{}_{old} + C_{ijkl}\Delta\varepsilon_{kl} \tag{8}$$

The value of the loading function f is evaluated by Eq. (6): if $f < 0$ a pure elastic deformation is occurring during the increment and the evaluated stress state is the correct stress state, if $f > 0$ the deformation is partly plastic and the elastic trial stress state must be corrected for plastic deformation such as:

$$\sigma_{ij}{}_{new} = \sigma_{ij}^{tr}{}_{new} - \Delta\lambda C_{ijkl}\frac{\partial f}{\partial \sigma_{kl}} \tag{9}$$

where $\Delta\lambda$ is the plastic multiplier increment given by:

$$\Delta\lambda = \frac{\frac{\partial f}{\partial \sigma_{ij}} C_{ijkl}\Delta\varepsilon_{kl}}{\frac{\partial f}{\partial \sigma_{ij}} C_{ijkl}\frac{\partial f}{\partial \sigma_{kl}} + \frac{\partial \sigma_y}{\partial \varepsilon_{eq}^p}_{ij}} \tag{10}$$

3.3 Homogenized Corrugated Cardboard Elastoplastic Model

A corrugated-core sandwich plate consists of a fluted corrugated sheet and two flat linerboards, where the fluting shape is defined with a sine function as:

$$\begin{cases} \theta(x) = \tan^{-1}\left(\dfrac{dh(x)}{dx}\right) \\ h(x) = \left(\dfrac{h_c}{2} - \dfrac{e_2}{2}\right)\sin\left(2\pi\dfrac{x}{P}\right) \end{cases} \tag{11}$$

where h_c is the distance between the linerboards, e_2 is the flute thickness and P is the fluting period defined in Fig. (5).

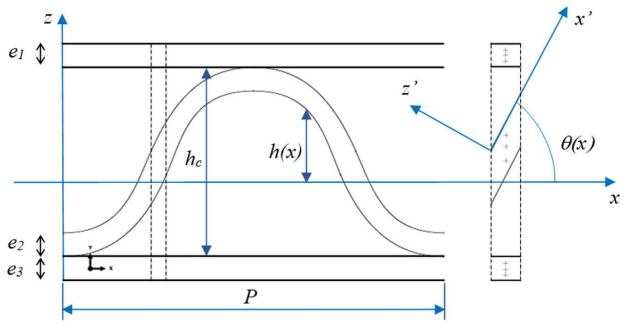

Fig. 5. Representation of the periodic unit cell for corrugated cardboard.

For the elastic homogenization, the classical lamination theory was modified to consider the corrugated sheet. The laminate in plane forces $\{N\}$, transverse shear forces $\{T\}$ and out of plane moments $\{M\}$ can be related to the deformations $\{\varepsilon\}$, $\{\gamma\}$ and the curvature $\{\kappa\}$ of the laminate by the following expression:

$$\begin{Bmatrix} N_x \\ N_y \\ N_{xy} \\ M_x \\ M_y \\ M_{xy} \\ T_x \\ T_y \end{Bmatrix} = \begin{bmatrix} A_{11} & A_{12} & 0 & B_{11} & B_{12} & 0 & 0 & 0 \\ A_{12} & A_{22} & 0 & B_{12} & B_{22} & 0 & 0 & 0 \\ 0 & 0 & A_{33} & 0 & 0 & B_{33} & 0 & 0 \\ B_{11} & B_{12} & 0 & D_{11} & D_{12} & 0 & 0 & 0 \\ B_{12} & B_{22} & 0 & D_{12} & D_{22} & 0 & 0 & 0 \\ 0 & 0 & B_{11} & 0 & 0 & D_{33} & 0 & 0 \\ 0 & 0 & 0 & 0 & 0 & 0 & F_{11} & 0 \\ 0 & 0 & 0 & 0 & 0 & 0 & 0 & F_{22} \end{bmatrix} \begin{Bmatrix} \varepsilon_x \\ \varepsilon_y \\ \gamma_{xy} \\ \kappa_x \\ \kappa_y \\ \kappa_{xy} \\ \gamma_{xz} \\ \gamma_{yz} \end{Bmatrix} \tag{12}$$

with:

$$\begin{cases} A_{ij}(x) = Q_{ij}^{(1)} e_1 + Q_{ij}^{(2)}(\theta(x)) \dfrac{e_2}{\cos\theta(x)} + Q_{ij}^{(3)} e_3 \\ B_{ij}(x) = Q_{ij}^{(1)} z_1 e_1 + Q_{ij}^{(2)}(\theta(x)) z_2 \dfrac{e_2}{\cos\theta(x)} + Q_{ij}^{(3)} z_3 e_3 \\ D_{ij}(x) = Q_{ij}^{(1)} \left(z_1^2 e_1 + \dfrac{e_1^2}{12} \right) + Q_{ij}^{(2)}(\theta(x)) \left(z_2^2 \dfrac{e_2}{\cos\theta(x)} + \dfrac{e_2^2}{12\cos^2\theta(x)} \right) \\ \qquad + Q_{ij}^{(3)} \left(z_3^2 e_3 + + \dfrac{e_3^2}{12} \right) \\ F_{ij}(x) = \dfrac{5}{6} \left(C_{ij}^{(1)} e_1 + C_{ij}^{(2)}(\theta(x)) \dfrac{e_2}{\cos\theta(x)} + C_{ij}^{(3)} e_3 \right) \end{cases} \tag{13}$$

where $Q_{ij}^{(k)}$ is the reduced stiffness matrix (Eq. (14)), $C_{ij}^{(k)}$ is the transverse shear stiffness matrix (Eq. (15)), and subscripts 1, 2 and 3 denote outer linerboard, inner linerboard and fluting, respectively.

$$[Q]^{(k)} = \begin{bmatrix} \frac{E_x}{1-\nu_{xy}\nu_{yx}} & \frac{\nu_{xy}E_y}{1-\nu_{xy}\nu_{yx}} & 0 \\ \frac{\nu_{yx}E_x}{1-\nu_{xy}\nu_{yx}} & \frac{E_y}{1-\nu_{xy}\nu_{yx}} & 0 \\ 0 & 0 & G_{xy} \end{bmatrix}^{(k)} \tag{14}$$

$$[C]^{(k)} = \begin{bmatrix} G_{yz} & 0 \\ 0 & G_{xz} \end{bmatrix}^{(k)} \tag{15}$$

where E_x, E_y, ν_{xy}, G_{xy}, G_{yz}, G_{xz} are the elastic material properties, with x, y, z the paperboard MD, CD and ZD directions, respectively.

The global equivalent stiffness matrix for elastic case is obtained by integrating Eq. (13) over a fluting period P:

$$\begin{cases} A_{ij}^h = \displaystyle\int_0^P A_{ij}(x)dx \\ B_{ij}^h = \displaystyle\int_0^P B_{ij}(x)dx \\ D_{ij}^h = \displaystyle\int_0^P D_{ij}(x)dx \\ F_{ij}^h = \displaystyle\int_0^P F_{ij}(x)dx \end{cases} \tag{16}$$

Some simplifying assumptions and detailed calculations of the equivalent stiffness terms can be found in [14-17].

The elastic parameters of linerboards and fluting are obtained from standard experimental tensile tests. Then, the homogeneous stiffnesses of corrugated cardboard are computed using Eq. (16). Finally, the homogenized material stiffness matrix Q_{ij}^h of the corrugated cardboard is obtained from Eq. (17):

$$Q_{ij}^h = \frac{12 D_{ij}^h}{t_h^3} \tag{17}$$

with:

$$t_h = \sqrt{\frac{\sum_{n=1}^{3} D_{nn}^h}{\sum_{n=1}^{3} A_{nn}^h}} \tag{18}$$

To find the effective elastoplastic parameters for shell model that replaces 3D structural corrugated cardboard model, an inverse identification procedure is used. We carried out three tensile test simulations on different samples: MD-sample, CD-sample and 45° oriented-sample using a 3D structural model to generate tensile curves, which are then used to identify an equivalent shell. The 3D structural and the 2D homogenized tensile samples are meshed with rectangular reduced integration shells elements (S4R) with a mesh size of 0.5 mm as shown in Fig. (6).

The obtained load vs displacement curves are compared to the numerical equivalent shell curves by minimizing the least square error defined in Eq. (19).

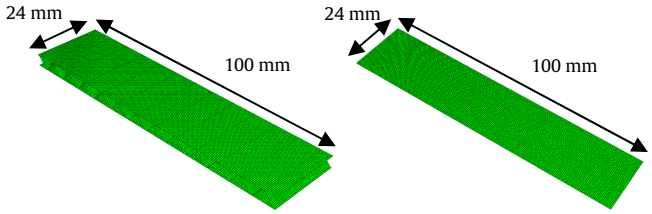

Fig. 6. Three-dimensional structural and equivalent corrugated cardboard meshes.

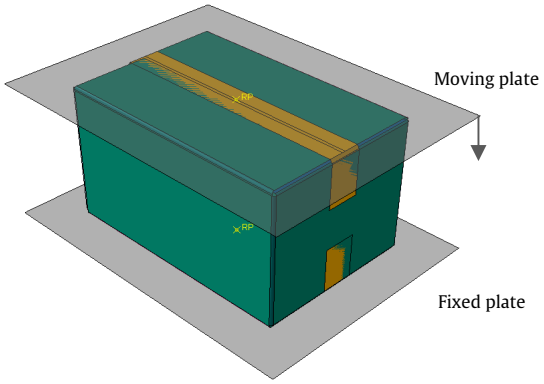

Fig. 7. Boundary conditions for box compression test.

$$F_{err} = \frac{1}{N}\sum_{i=1}^{N}\left(F_h(\{P\}, t_i) - F_{3D}(t_i)\right)^2 \tag{19}$$

where F_h and F_{3D} are the equivalent shell and 3D structural numerical forces at t_i sampling point, respectively, $\{P\} = \{E_0, \varepsilon_0, n, a, b, c, d\}$ is the unknown parameter vector and N is the number of sampling points.

The nonlinearity of the objective function and the possibility of non-uniqueness of the solution make the inverse problem a nonconvex optimization problem. Therefore, a robust global optimization method was required. In this study, the Multi-Objective Genetic Algorithm (MOGA-II) [30-31] was used. It uses a smart multisearch elitism for robustness and directional crossover for fast convergence. Its efficiency is ruled by its operators (classical crossover, directional crossover, mutation and selection) and by the use of elitism. In this study, we used the following parameters: population size = 12, Probability of Directional Cross-over = 0.5, Probability of Selection = 0.05, Probability of Mutation = 0.1, and number of generations = 20.

4. Results and Discussion

4.1 Model Calibration

We used the method proposed in previous section to evaluate the equivalent elastoplastic parameters of the corrugated cardboard as follows:

- Evaluation of the linerboards and the fluting elastic properties from the experimental tensile tests. The obtained properties are given in Table (2).
- Simulation of three tensile tests on different samples (MD, CD and 45°) using a 3D structural model to generate tensile curves.
- Identification of the equivalent elastoplastic parameters of the corrugated cardboard using inverse analysis procedure by comparing the generated tensile curves with the simulation tensile curves obtained using the homogenized shell.

The determined equivalent elastoplastic parameters of the corrugated cardboard are summarized in Table (3).

The identified model is finally used to simulate the box compression test presented in section (2.3). The finite element model consists of two rigid plates that transmit loads to the box and which size is the same as experiment (Fig. (7)). For this simulation friction interaction between plates and box was used to model boundary conditions of system. Bottom rigid plate is fixed so it serves as support for box and top plate is moved vertically for a given displacement. Furthermore, the displacements and rotations of top plate is constrained in other directions. The box is meshed using 9603 rectangular reduced integration shell elements (S4R) and 10152 nodes.

Table 2. Elastoplastic properties of linerboards and fluting.

	E_x (MPa)	E_y (MPa)	ν_{xy}	G_{xy} (MPa)	E_0 (MPa)	n	a	b	c	d	ε_0
Top linerboard	3008	1505	0.17	834	256	2.03	1	2.03	2.28	1.18	0.0034
Fluting	3072	1454	0.15	705	436	1.62	1	2.01	1.25	1.13	0.0010
Bottom linerboard	3034	1502	0.23	737	184	2.06	1	2.21	2.19	1.32	0.0011

Table 3. Equivalent elastoplastic properties of the corrugated cardboard.

E_x^h (MPa)	E_y^h (MPa)	ν_{xy}^h	G_{xy}^h (MPa)	E_0^h (MPa)	n^h	a^h	b^h	c^h	d^h	ε_0^h
368.8	351.8	0.092	166.2	38.5	2.04	1	1.65	0.84	1.55	0.0068

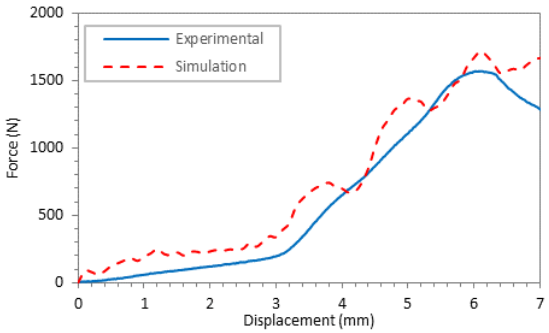

Fig. 8. Comparison of numerical and experimental box compression test curves.

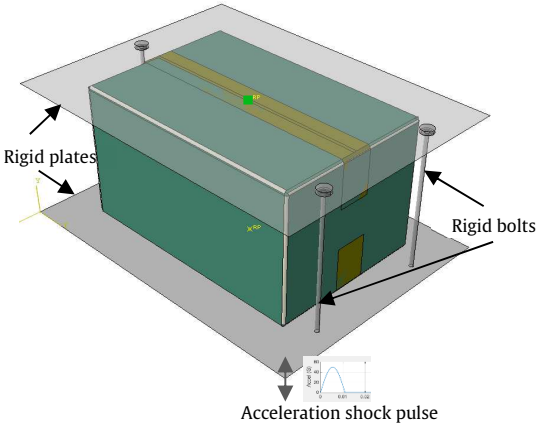

Fig. 9. Boundary conditions for shock test.

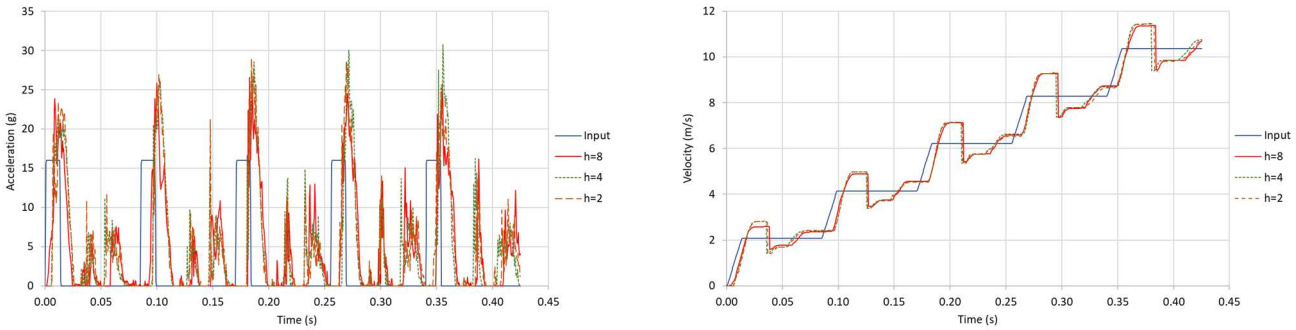

(a) (b)

Fig. 10. Effect of mesh refinement on variable responses recorded at top rigid plate: (a) acceleration and (b) velocity.

Figure (8) shows the comparison of the experimental and numerical compression curves of the box with a good agreement. The maximum load obtained by the homogenized model is 1716.8 N compared to the experimental value of 1569.1 N giving a relative difference of 9.4%.

4.2 Repetitive Shock Results

For the simulation of shock test, the finite element model consists of a box placed between two rigid plates connected by rigid bolts as shown in Fig. (9). Top plate has a mass of 8.4 kg as in experimental test and is free to move only vertically. An acceleration shock pulse is applied to the bottom rigid plate for a short time. Acceleration and velocity change are recorded on the bottom plate during the simulations. For this simulation friction interaction between plates and box was used to model boundary conditions of system.

To replicate the experimental fatigue shock tests, simulations of successive shock pulses are carried out until the box is damaged. The box is considered damaged when the equivalent plastic strains exceeds 5%.

To gain confidence in the accuracy of our model, we solved the model on progressively finer meshes and compared results. Since we need the accelerations and the velocity variations to plot DBC, we have plotted in Fig. (10) the results obtained for five successive shocks for three mesh refinements (h=8, 4, 2 mm) in the case of acceleration shock pulse of 16g and shock duration of 14.2 ms. The acceleration and velocity responses recorded at top rigid plate show similar trends for the three meshes, but the amplitudes are closer for the meshes h = 4 mm and h = 2 mm. We have also plotted various model energies for the three meshes in Fig. (11). As we perform a dynamic calculation, the internal and kinetic energies change over time (Figs. 11(a) and 11(b)). Figure 11(c) shows also the energy dissipated by plasticity. The energy balance for the three meshes is shown in Fig. 10(d) which should be constant. However, in the numerical model this is only approximately constant, generally with an error of less than 1% which is the case in our simulations. After this sensitivity analysis, we selected the mesh h = 4 mm for relevant computations while keeping a reasonable computational cost.

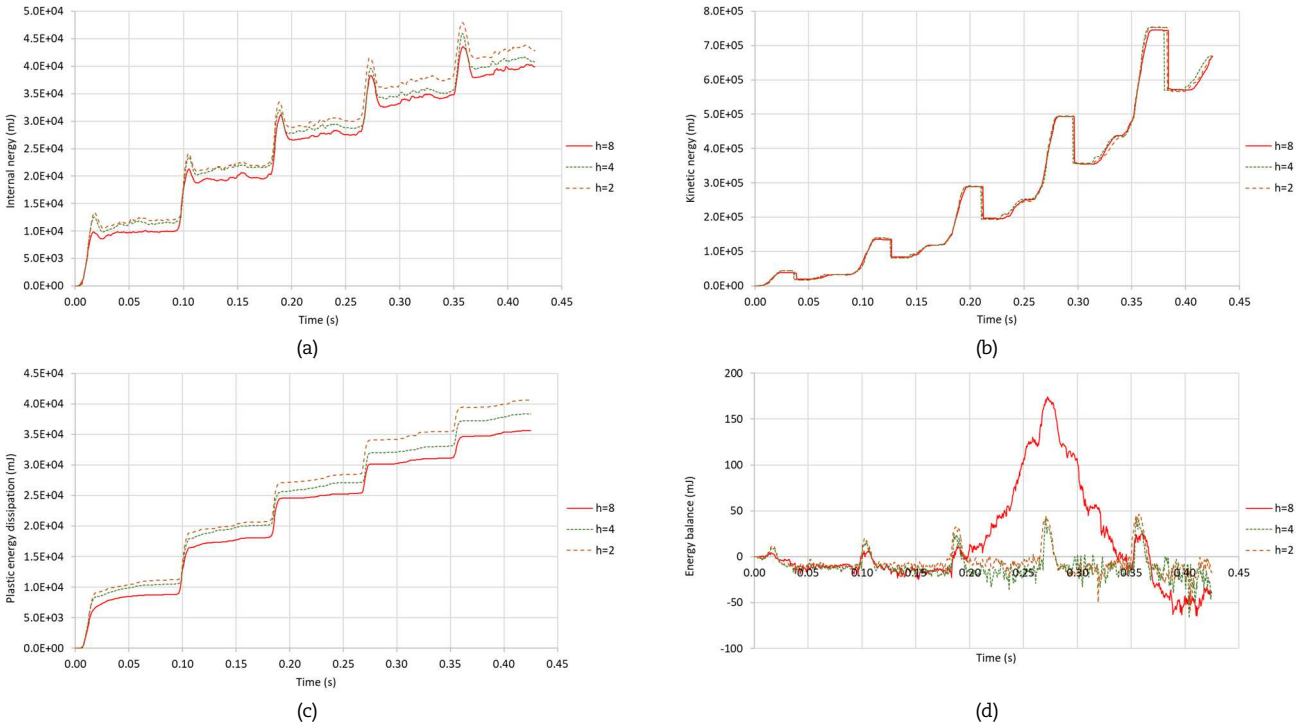

Fig. 11. Effect of mesh refinement on various model energies: (a) Internal energy, (b) Kinetic energy, (c) Plastic energy dissipation and (d) Energy balance .

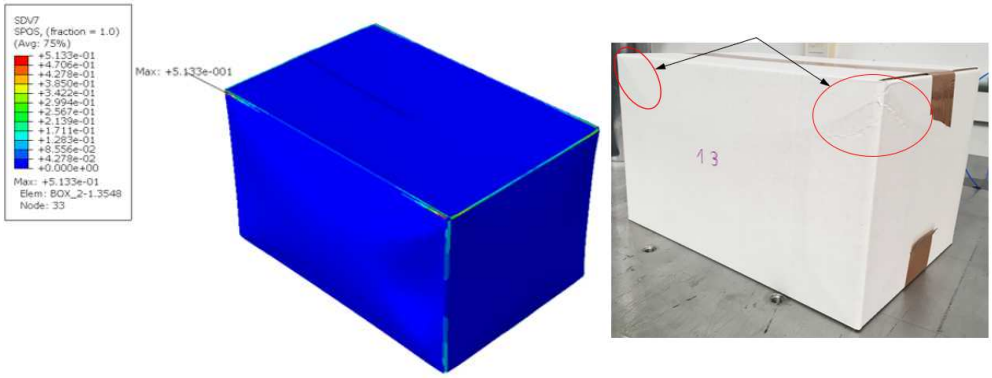

Fig. 12. Numerical and experimental damaged box.

Low fatigue cycle, also called “Oligocyclique Fatigue”, is characterized by high stress and low fatigue life. For the limited endurance fatigue, lifetime is intermediate and varies rapidly in function of applied stress. For unlimited endurance fatigue, the lifetime is infinite.

In this study, for oligocyclique and limited endurance fatigue, the number of shocks necessary for the box to damage is determined directly from the Abaqus simulations since the number of cycles is low. However, the number of cycles to damage the box can be very high and it is practically not feasible to perform a cycle-by-cycle simulation. To reduce computational costs, we propose a simple method consisting in extrapolating the equivalent plastic strain after some training cycles. This method is based on a trend line, established during finite element analysis for training cycles. This trend is used to extrapolate the remaining cycles.

For oligocyclique fatigue, damage of the box is observed after the first shock both experimentally and numerically as shown in Fig. (12).

For limited endurance fatigue, damage of the box is observed after several shocks given in Table (4). We can see that our numerical model gives the same order of magnitude as the experimental results.

For the unlimited endurance fatigue, we stopped experimental testing after a thousand shocks considering that the box reaches the unlimited endurance zone. We compare in Table (5) shock numbers for box to undergoes damage obtained for experimental tests and with the extrapolation method. Despite the various simplifying assumptions, the proposed model gives satisfactory results.

Figure (13) represents the experimental and numerical damage boundary curve of the studied box that define its fragility based on its sensitivity to acceleration and the that occurs during shock.

To compare the velocity change experimental and simulation results, Figs. 14(a) and 14(b) display experimental and simulation frequency distribution for grouped data. The distributions are asymmetric and positively skewed, the values tend to cluster toward the lower end of the scale. Hence, in these sets of points, the mean is higher than the median because the latter is dragged in the direction of the tail. Figs. 14(c) and (d) show a good comparison of the approximated Probability Density Function (PDF) and Cumulative Distribution Function (CDF) of experimental and numerical velocity change variables.

Table 4. Number of shocks for limited endurance fatigue.

Acceleration (g)	Shock duration (ms)	Experimental shock number	Numerical shock number
17	13.7	4	2
14	17.0	7	10
20	13.5	2	2
14	16.2	9	13
14	17.2	8	11
15	15.9	4	2
16	13.3	36	20
16	14.2	3	5
18	13.9	4	1
17	14.2	3	1
17	14.4	2	1
19	14.1	3	1
31	7.8	3	3
45	6.65	2	1

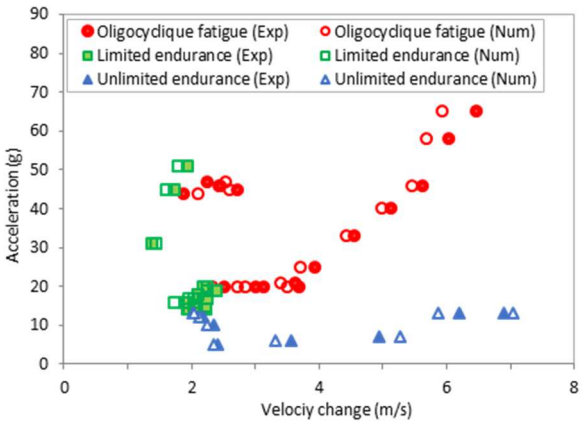

Fig. 13. Comparison of experimental and numerical shock fatigue results.

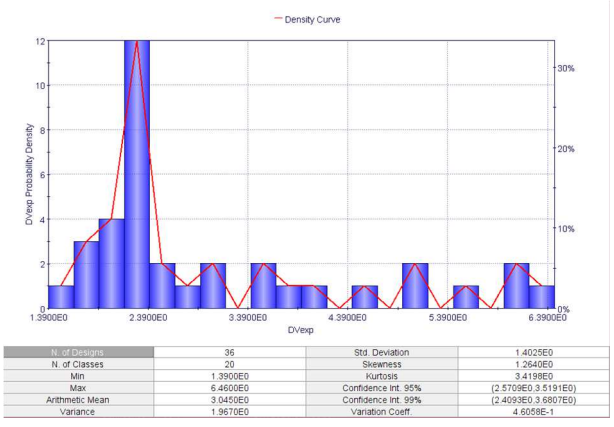

(a) Experimental results PDF

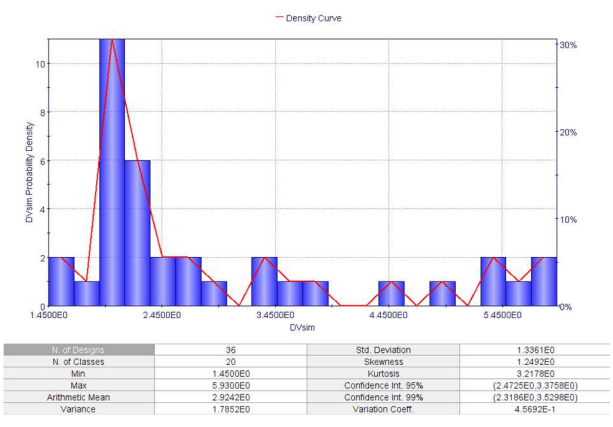

(b) Numerical results PDF

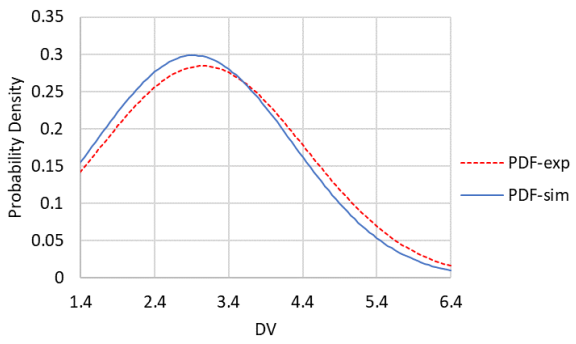

(c) PDF

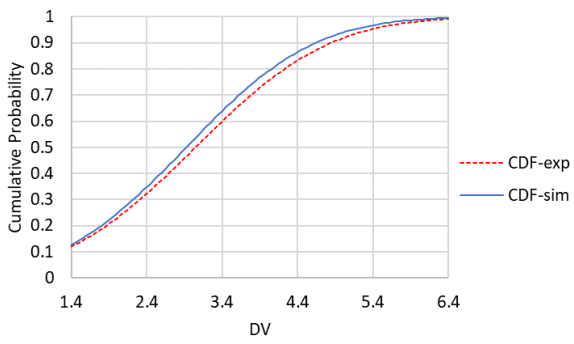

(d) CDF

Fig. 14. Statistical comparison of experimental and numerical shock fatigue results.

Table 5. Number of shocks for unlimited endurance fatigue.

Acceleration (g)	Shock duration (ms)	Experimental shock number	Numerical shock number
5	49.8	>1000	1740
12	20.1	>1000	600
10	25.0	>1000	1273
13	17.1	>1000	420
6	59.4	>1000	1505
7	80.8	>1000	1160
13	48.7	>1000	140

5. Conclusion

In present work, the effect of shock fatigue on corrugated cardboard boxes was estimated by vibration table and finite element methods. The damage boundary curve of the studied box, that define its fragility based on its sensitivity to acceleration and the velocity change that occurs during shock, was constructed using both methods. To efficiently simulate the mechanical behavior of a corrugated cardboard box, we proposed an elastoplastic homogenization model to replace a corrugated-core sandwich panel by a homogeneous plate. The proposed model performs satisfactorily in static and dynamic loading. Experimental characterization can be time-consuming and expensive. We have showed that it is possible to estimate DBC of the package using finite element method with good precision. This technique can easily be applied to other packaging. However, the physical testing is still needed to validate the final design.

Author Contributions

V.D. Luong carried out the simulations; A.-S. Bonnin and J.-B. Nolot conducted the experiments and analyzed the experimental results; D. Erre designed the experiments and analyzed the experimental results; F. Abbès and B. Abbès developed the mathematical modeling and examined the theory validation. The manuscript was written through the contribution of all authors. All authors discussed the results, reviewed, and approved the final version of the manuscript.

Conflict of Interest

The authors declared no potential conflicts of interest with respect to the research, authorship, and publication of this article.

Funding

The authors received no financial support for the research, authorship, and publication of this article.

References

[1] Goodwin, D., Young, D., *Protective packaging for distribution*, DEStech Publications, Lancaster, PA, USA, 2011.
[2] Newton, R.E., *Fragility Assessment Theory and Practice*, Monterey Research Laboratory, Inc., California, 1976.
[3] Burgess, G.J., Product fragility and damage boundary theory, *Packaging Technolgy and Science*, 1(1), 1988, 5– 10.
[4] Kipp, W.I., Developments in testing products for distribution, *Packaging Technology and Science*, 13(3), 2000, 89– 98.
[5] Kitazawa, H., Saito, K., Ishikawa, Y., Effect of difference in acceleration and velocity change on product damage due to repetitive shock, *Packaging Technology and Science*, 27(3), 2014, 221-230.
[6] Horiguchi, S., Saito, K., Test method for enhanced mechanical shock fragility statistics accuracy, *Packaging Technology and Science*, 32(4), 2019, 199-210.
[7] Luong, V.D., Abbès, F., Abbès, B., Duong, P.T.M., Nolot, J.-B., Erre, D., Guo, Y.-Q., Finite element simulation of the strength of corrugated board boxes under impact dynamics, *In: Nguyen-Xuan H., Phung-Van P., Rabczuk T. (eds) Proceedings of the International Conference on Advances in Computational Mechanics 2017, ACOME 2017, Lecture Notes in Mechanical Engineering*, 2018, 369-380.
[8] Li, H., Chen, A., Duan, N., Dropping Shock Characteristics of the Suspension Cushioning System with Critical Components, *Shock and Vibration*, 2017, 2017, 3164294.
[9] Song, S., Duan, N.-N., Chen, A.-J., Application of variational iteration method for dropping damage evaluation of the suspension spring packaging system, *Abstract and Applied Analysis*, 2014, 2014, 385404.
[10] Biancolini, M.E., Brutti, C., Numerical and experimental investigation of the strength of corrugated board packages, *Packaging Technology and Science*, 16(2), 2003, 47-60.
[11] Biancolini, M.E., Brutti, C., Porziani, S., Corrugated board containers design methods, *International Journal of Computational Materials Science and Surface Engineering*, 3(2-3), 2010, 143-163.
[12] Han, J., Park, J.M., Finite element analysis of vent/hand hole designs for corrugated fibreboard boxes, *Packaging Technology and Science*, 20(1), 2007, 39- 47.
[13] Fadiji, T., Coetzee, C., Opara, U.L., Compression strength of ventilated corrugated paperboard packages: numerical modelling, experimental validation and effects of vent geometric design, *Biosystems Engineering*, 151, 2016, 231-247.
[14] Duong, P.T.M., Abbès, B., Li, Y.M., Hammou, A.D., Makhlouf, M., Guo, Y.-Q., An analytic homogenization model for shear torsion coupling problems of double corrugated core sandwich plates, *Journal of Composite Materials*, 47(11), 2013, 1327–1341.
[15] Hammou, A.D., Duong, P.T.M., Abbès, B., Makhlouf, M., Guo, Y.-Q., Finite element simulation with a homogenization model and experimental study of free drop tests of corrugated cardboard packaging, *Mechanics & Industry*, 13(3), 2012, 175–184.
[16] Abbès, B., Guo, Y.-Q., Analytic homogenization for torsion of orthotropic sandwich plates: application to corrugated cardboard, *Composite Structures*, 92(3), 2010, 699–706.
[17] Talbi, N., Batti, A., Ayad, R., Guo, Y.-Q., An analytical homogenization model for finite element modeling of corrugated cardboard, *Composite Structures*, 88(2), 2009, 280–289.
[18] Nordstrand, T., Carlsson, L.A., Allen, H.G., Transverse shear stiffness of structural core sandwich, *Composite Structures*, 27(3), 1994, 317–329.
[19] Garbowski, T., Marek, A., Homogenization of corrugated boards through inverse analysis, *An International Conference on Engineering and Applied Sciences Optimization, M. Papadrakakis, M.G. Karlaftis, N.D. Lagaros (eds.)*, Kos Island, Greece, 4-6, June 2014.
[20] Rabczuk, T., Kim, J. Y., Samaniego, E., Belytschko, T., Homogenization of sandwich structures, *International Journal for Numerical Methods in Engineering*, 61, 2004, 1009–1027.
[21] Anitescu, C., Atroshchenko, E., Alajlan, N., Rabczuk, T., Artificial Neural Network methods for the solution of second order boundary value problems, *Computers, Materials and Continua*, 59(1), 2019, 345-359.
[22] Hill, R., A theory of the yielding and plastic flow in anisotropic metals, *Proceedings of The Royal Society*, 193, 1948, 111–128.
[23] Hoffman, O., The brittle strength of orthotropic materials, *Journal of Composite Materials*, 1(2), 1967, 200–206.
[24] Tsai, S.W., Wu, E.M., A general theory of strength for anisotropic materials, *Journal of Composite Materials*, 5(1), 1971, 58–80.

[25] Xia, Q.S., Boyce, M.C., Parks, D.M., A constitutive model for the anisotropic elastic-plastic deformation of paper and paper board, *International Journal of Solids and Structures*, 39(15), 2002, 4053-4071.
[26] Mäkelä, P., Östlund, S., Orthotropic elastic-plastic material model for paper materials, *International Journal of Solids and Structures*, 40(21), 2003, 5599-5620.
[27] Harrysson, A., Ristinmaa, M., Large strain elasto-plastic model of paper and corrugated board, *International Journal of Solids and Structures*, 45(11-12), 2008, 3334–3352.
[28] Karafillis, A.P., Boyce, M.C., A general anisotropic yield criterion using bounds and a transformation weighting tensor, *Journal of the Mechanics and Physics of Solids*, 41(12), 1993, 1859–1886.
[29] Abaqus v. 6.19 documentation, Dassault Systemes Simulia Corporation, 2016.
[30] Poloni C., Pediroda, V., GA coupled with computationally expensive simulations: tools to improve efficiency, *In Genetic Algorithms and Evolution Strategies in Engineering and Computer Science*, John Wiley and Sons, England, 1997.
[31] Spicer, D., Cook, J., Poloni C., Sen P., EP20082 Frontier: Industrial MultiObjective Design Optimisation, *In Proceedings of the 4th European Computational Fluid Dynamics Conference (ECCOMAS 98)*, John Wiley and Sons, England, 1998.

ORCID iD

Fazilay Abbès https://orcid.org/0000-0003-0036-822X
Boussad Abbès https://orcid.org/0000-0003-1192-6549

How to cite this article: Luong V.D., Bonnin A.-S., Abbès F., Nolot J.-B., Erre D., Abbès A. Finite element and experimental investigation on the effect of repetitive shock in corrugated cardboard packaging, *J. Appl. Comput. Mech.*, 7(2), 2021, 820–830. https://doi.org/10.22055/JACM.2020.35968.2771